

AN OUT-OF-PLANE MEMS QUADRUPOLE FOR A PORTABLE MASS SPECTROMETER

L. F. Velásquez-García¹, and A.I. Akinwande²

¹ Microsystems Technologies Laboratories, Massachusetts Institute of Technology, Cambridge MA, USA
(Tel: 1 617 253 – 0730, E-mail: lfvelasq@mit.edu)

² Department of Electrical Engineering and Computer Science, Massachusetts Institute of Technology, Cambridge MA, USA
(Tel: 1 617 258 – 7974, E-mail: akinwand@mtl.mit.edu)

Abstract: This paper reports the design, fabrication and characterization of a hand-assembled out-of-plane MEMS quadrupole mass filter. The device utilizes a 3D packaging technology that relies on mesoscale DRIE-patterned deflection springs for assembly. Microfabricated quadrupoles with 1.58 mm down to 0.56 mm diameter rods and 30 to 60 aspect ratios were built and tested. The quadrupoles were characterized in the first stability region at an RF frequency of 1.44 MHz, using a constant peak width sweeping method, obtaining a dynamic range of 650 amu and a half-peak width of 2 amu. Better performance is expected if a higher RF frequency is used.

Keywords: mass filter, out-of-plane quadrupole, portable mass spectrometry.

1. INTRODUCTION

A quadrupole is a set of four electrodes in a symmetric configuration that can filter charged species using a combination of constant and time-varying electric potentials [1]. Fig. 1 shows the cross-section of a quadrupole with circular electrodes. The electrodes with radius r are tangential to a circle with radius r_o . Opposite electrodes are biased at the same potential. The optimal r/r_o ratio for mass filtering is 1.148 [2].

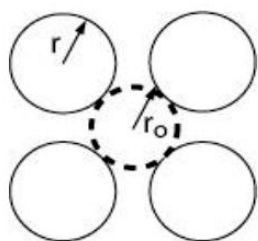


Fig. 1 Circular rod quadrupole cross-section.

The dynamics of a charged particle inside the quadrupole are described by the Mathieu equation

$$\frac{d^2 u}{d\xi^2} + [a_u - 2q_u \cos(2\xi)]u = 0 \quad (1)$$

where u is x or y –the orthogonal directions of the plane perpendicular to quadrupole axis, ξ is the

dimensionless time $\omega t/2$, and a_u and q_u are the dimensionless Mathieu parameters

$$a_u = a_x = -a_y = \frac{8q^*U}{r_o^2\omega^2} \quad (2)$$

$$q_u = q_x = -q_y = \frac{4q^*V}{r_o^2\omega^2} \quad (3)$$

where q^* is the specific charge of the particle, U is the magnitude of the DC voltage, and V is the amplitude of the RF voltage with angular frequency ω .

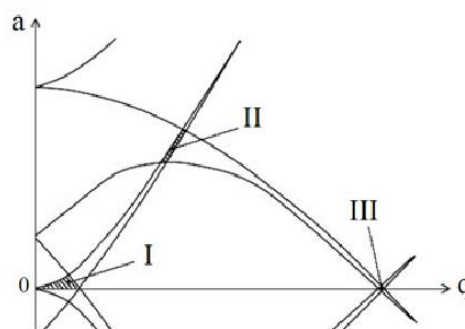


Fig. 2 First, second and third stability regions.

For each orthogonal direction there is a family of regions in the (a, q) plane where the Mathieu parameters imply a stable confinement of the charged particle. The intersection of the two

families defines the stability regions, i.e., set of Mathieu parameters that will result in the confinement of the particle within the quadrupole and thus be transmitted (Fig. 2). The operational (a, q) point fixes the DC-to-RF amplitude ratio of the electric potential. The results reported in this paper are from quadrupoles operating in the first stability region.

The quadrupole resolution R is defined as

$$R = m / \Delta m \quad (4)$$

where Δm is the half width of the peak centered around mass m . In terms of the stability diagram, higher resolution is obtained if the quadrupole is operated with an (a, q) that falls near an apex of the stability region. Variations in mass resulting in perturbations of the a and q values will readily put the system outside the stability region. The first stability region has an apex with a and q values equal to 0.2346 and 0.7037 respectively. Experimentally, it has been reported that the resolution is proportional to the square of the number of RF cycles n that a charged particle spends within the quadrupole

$$R \cong n^2 / h \quad (5)$$

where h is a constant dependent on the stability region and experimental setup. Typical h -values of 10 to 20 have been used for the first stability region [1].

There has been an active interest in developing scaled-down quadrupole technology for over a decade. Miniaturized quadrupoles [3, 4], and MEMS in-plane quadrupoles have been reported [5, 6]. The novelty of the device that we report resides in its out-of-plane configuration that makes it easier to integrate with in-line ion sources and detectors because they emit/sense perpendicular to the substrate surface. Also, the quadrupole is designed as a flexible research tool where sets of rods with different lengths can be easily swapped without loss of resolution or sensitivity, and electrostatic optics could be readily added to the quadrupole basic assembly.

This paper reports a proof of concept quadrupole mass filter, which is part of a portable mass spectrometer in a gas detection system dubbed the Micro-Gas Analyzer (MGA). The

system architecture of the mass spectrometer is shown in Fig. 3 and it consists of a carbon nanotube (CNT) ionizer array, an array of MEMS electrometers for species detection, and a micro-pump to provide the required vacuum level.

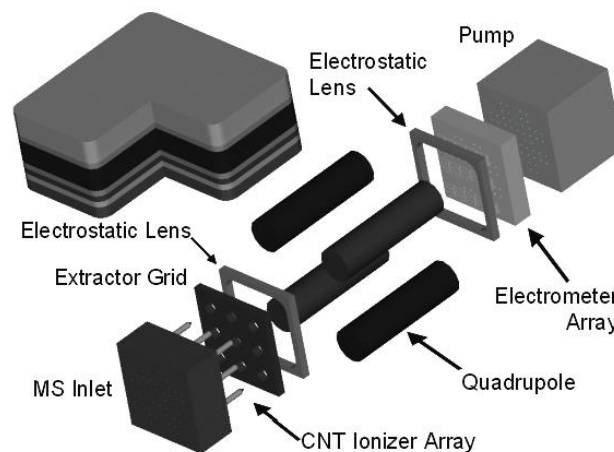


Fig. 3 System architecture of a portable MEMS-based mass spectrometer.

2. QUADRUPOLE DESIGN

Scaling down quadrupoles enables device portability and higher operational pressure. The volume and weight of the device is dominated by the electrodes, which will scale as the cube of the rod diameter for a given aspect ratio. For proper operation, the electrode length should be smaller than λ —the mean-free path of the background gas, which is inversely proportional to its pressure. As reference, λ for air at 1 mTorr and room temperature is about 5 cm.

Operation of the quadrupole at a higher pressure positively impacts the pumping subsystem as well. On the one hand, there is no vacuum technology that can work between two arbitrary pressure levels. As the lower pressure bound decreases, the pump subsystem will need to include additional pumping schemes thus adding hardware complexity and power consumption. On the other hand, it can be readily shown from first principles that the minimum power W required to bring an ideal gas from pressure P_2 to P_1 is [7]

$$W = \oint P dV = \frac{\alpha}{1-\alpha} \dot{m} \cdot R \cdot T_1 \left[\left(\frac{P_2}{P_1} \right)^{\frac{\alpha-1}{\alpha}} - 1 \right] \quad (6)$$

where \dot{V} is the volume flowrate, α is the polytropic coefficient of the cycle ($1 < \alpha < \gamma$, γ is the ratio between the heat coefficient at constant pressure to the heat coefficient at constant volume), \dot{m} is the mass flowrate, T_i is the gas temperature at the low-pressure bound, and the pressure ratio P_2/P_1 is larger than unity. Therefore, a higher low-pressure bound implies a smaller pressure ratio, which requires less power.

The design of a quadrupole with a given resolution is dominated by the lower bound of the mass range and the performance of the ionizer. The number of cycles n that a charged particle of mass m spends within the quadrupole is

$$n = f \cdot \frac{L}{v_z} = f \cdot L \sqrt{\frac{m}{2 \cdot E_z}} \quad (7)$$

where L is the quadrupole length, f is the RF frequency, v_z is the axial ion velocity, and E_z is the axial ion energy. Clearly, the minimum number of cycles is set by the lower bound of the mass range. Therefore, it can be shown using Eq. (3), (5) and (7) that the minimum rod aspect ratio is

$$\frac{L}{D}_{\min} \approx \frac{\pi}{1.62} \sqrt{\frac{R \cdot E_z \cdot q_u \cdot h}{e \cdot V_{\min}}} \quad (8)$$

where D is the rod diameter, e is the charge of the particle, and V_{\min} is the smallest RF amplitude that the power supply can accurately deliver –the amplitude used to scan the lower bound of the mass range. Eq. (8) predicts the maximum rod diameter for a given pressure level ($L \leq \lambda$). From Eq. (3) the driving frequency is then

$$f = \frac{2.3}{\pi D} \sqrt{\frac{e \cdot V_{\min}}{m_{\min} \cdot q_u}} \quad (9)$$

The ratio between the RF amplitude and the particle mass is constant for f and q_u constant. The bias voltage needed to resolve the upper bound of the mass range should be smaller than the breakdown voltage of the quadrupole.

However, there are also disadvantages when scaling down, thus preventing an arbitrarily small quadrupole. Adverse effects include smaller signal-to-noise ratio for a fixed ion current flux, added RF circuit complexity to achieve higher frequencies, lower RF power transfer efficiency, and decrease in performance due to the impact of

dimensional non-idealities [8]. The discussion of these effects is outside the scope of this manuscript.

3. THE μ GRIPPER

The μ Gripper is a micro-fabricated quadrupole platform that uses silicon DRIE-patterned deflection springs to precisely aid the hand-assembly of MEMS quadrupoles. It uses a packaging approach that allows the assembly of sub-systems of a device with incompatible process flows or low yield [9]. The technology has a measured biaxial assembly precision of about 5 μ m with sub-micron repeatability [10].

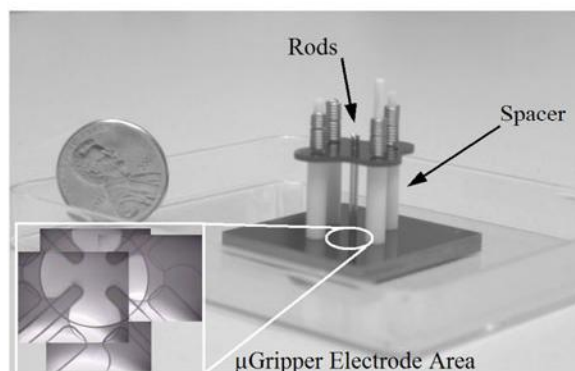


Fig. 4 A MEMS quadrupole assembled using a μ Gripper, near a 1-cent US coin for reference.

Fig. 4 shows a MEMS quadrupole with 0.56 mm diameter rods and aspect ratio of 55. The quadrupole assembly utilizes two microfabricated pieces –a top aligning plate, and a springhead base, i.e., the μ Gripper. A set of ceramic spacers, and dowel pins with 5 μ m diameter precision are also needed to complete the quadrupoles. The μ Gripper is 3 cm \times 3 cm \times 3 mm with spacer holes near the corners, and electrode holes near the center. This platform can accommodate 0.56 to 1.58 mm diameter rods of any aspect ratio.

Fig. 5 shows a cross-section of the four silicon layers of the μ Gripper. The core of the device is the Upper Middle wafer that has the deflection springs. The Top and Lower Middle wafers are mirror images except that the top wafer is thicker. These two wafers have recesses that surround the deflection springs to ensure smooth actuation, and through holes for the quadrupole rods and spacers.

The Bottom wafer has a set of through holes for ion transmission and the spacer assembly.

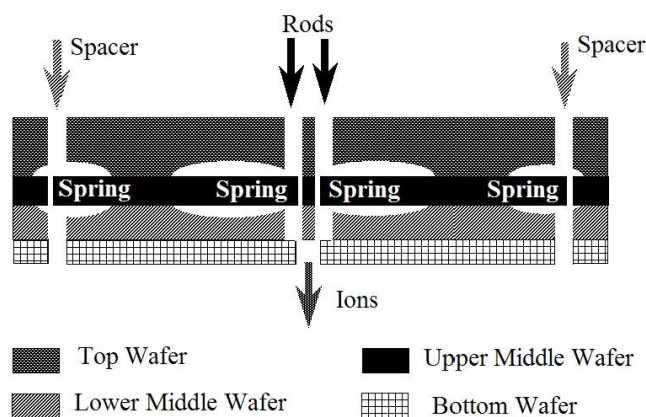


Fig. 5 Cross section schematic of the μ Gripper

The μ Gripper has two springs per rod with each spring controlling a different axis (Fig. 6). The same approach is used to position the spacers. The springs were designed for a maximum tensile stress of 150 MPa at a displacement of 200 μ m while producing a force of about 1 N [9]. The quadrupoles are assembled by inserting the 45° chamfered rods with a twisting motion to deflect the springs while setting the spring bodies in tension (no buckling) in case any frictional effects were present. The Bottom wafer stops the advance of the rods, providing proper vertical positioning.

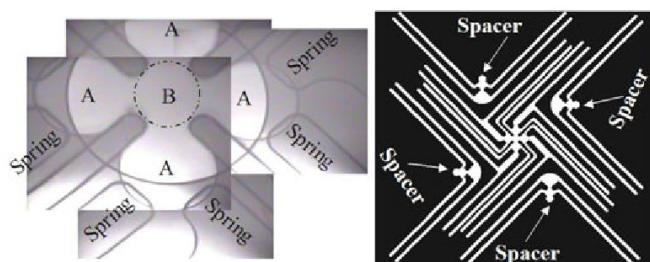


Fig. 6 Set of IR pictures of the μ Gripper central area (left), and complete spring layout (right). The electrodes occupy the cavities (A) that surround the ion transmission zone (B).

4. FABRICATION

Two process flows that use 6-inch, 10 – 20 Ω -cm Boron doped Silicon wafers produced the parts needed in the quadrupole assembly. The first process flow describes the fabrication of the top

aligning plate, while the second flow describes the μ Gripper fabrication.

4.1 Plate Process Flow

The top aligning plate uses 1000 ± 5 μ m thick substrates. The wafers are spin-coated with 10 μ m thick photoresist on one side, and contact photolithography is used to transfer the patterns to the aligning plates. The wafers are mounted on a handle wafer using photoresist, followed by a through-wafer DRIE-etch to form the pieces. The plates are dismantled from the handle wafer using an acetone soak. Finally, the aligning plates are RCA cleaned and wet oxidized @ 1050°C to grow a 2 μ m thick insulating layer.

4.2 μ Gripper Process Flow

The device is composed of four wafers, as shown in Fig. 7. The Top and Upper Middle wafers are 1000 ± 5 μ m thick, while the Lower Middle and Bottom wafers are 500 ± 5 μ m thick. The process flow of all μ Gripper wafers starts with an RCA clean and a growth of 0.3 μ m of thermal dioxide to protect the bonding surfaces. Each surface of the wafers is spin-coated with 1 μ m thick photoresist and contact photolithography is conducted to transfer the alignment marks. The features are patterned by reactive ion etching (RIE) of the silicon dioxide film and 0.5 μ m of the silicon substrate. The photoresist film is stripped with a piranha bath followed by the deposition of a 4 μ m thick PECVD silicon dioxide film on one side of the wafers. The film is annealed at 950°C for one hour in a nitrogen atmosphere. Subsequent process steps are as follows:

4.2.1 Top wafer / Lower Middle wafer: Both sides of the wafers are spin coated with 10 μ m thick photoresist and exposed using contact photolithography. The photoresist on top of the PECVD SiO₂ is patterned with the through-holes for the rods, spacers and transmission zone, while the photoresist film on other surface is patterned with the recesses that surround the deflection springs. Then, the oxide layers on both surfaces are etched using RIE. The recesses are etched using an SF₆ plasma to produce 5- μ m deep cavities. The wafers are then flipped over and attached to a quartz handle wafer using

photoresist. The through-holes are then etched using a DRIE step.

4.2.2 Upper Middle wafer / Bottom wafer: The side with the PECVD silicon dioxide film is spin-coated with 10 μm thick photoresist and exposed using contact photolithography. The Upper Middle wafer is patterned with the deflection springs, while the Bottom wafer is patterned with the spacers and transmission through-holes. After developing the resist films, the oxide film is etched using RIE. The wafers are then attached to a quartz handle wafer using photoresist, and the patterns are etched through the wafers with a DRIE step.

4.2.3 Final processing: The wafers are dismantled from the handle wafers using acetone and then piranha cleaned. The wafers are RCA cleaned and the oxide films on all surfaces are stripped using a 49% HF bath. The silicon wafers are then directly bonded at atmospheric pressure with 2500 N of force and held for at least 12 hours. The bonded stack is annealed at 1050°C for one hour in a nitrogen atmosphere. A 2 μm thick thermal silicon dioxide film is grown on the wafer stack before being die-sawed. Fig. 7 shows an IR picture of a wafer stack with 12 devices at near 100% yield.

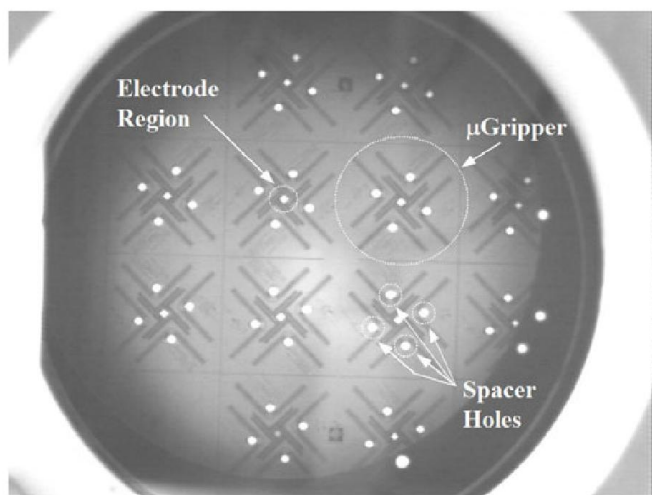


Fig. 7 IR picture of a $\mu\text{Gripper}$ wafer stack.

5. CHARACTERIZATION

The test rig included a chamber capable of vacuum levels below 10^{-7} Torr, an ion source, a channeltron, RF and DC power supplies and a controller. The thermionic ion source was made

by Ar dara Technologies (Ardara, PA), and produced 5 ± 1 eV ions. The RF power supply has an LC tank tuned to a specific frequency, taking into consideration the capacitive load of the quadrupole. An external circuit mixes the DC and RF signals. Electrical contact to the quadrupole electrodes was made using self-cleaning pogo pins from Everett Charles Technologies (Pomona, CA). The ionizer, power supplies, inlet and exit lenses are driven by a Merlin[®] automation data system and controllers made by Extrel (Pittsburgh, PA). The system also collects the channeltron signal through a preamplifier and a 12.5 kHz data acquisition board. A schematic of the test rig is shown in Fig. 8.

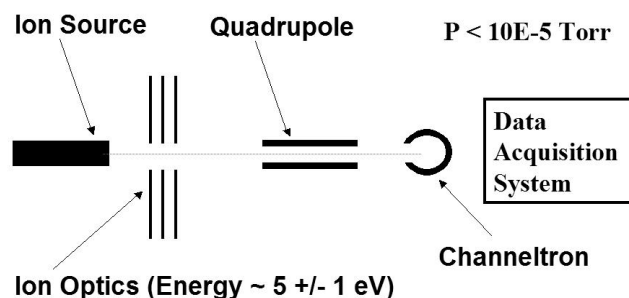


Fig. 8 Schematic of the quadrupole test setup.

The experimental procedure is as follows: The quadrupole and test jig are assembled, placed inside the vacuum chamber, and pumped to 10^{-6} Torr or lower. Air or Perfluorotributylamine vapor (FC-43) from Scientific Instrument Services, Inc. (Ringoos, NJ), is introduced into the vacuum chamber and stabilized at a pressure of about 10^{-5} Torr. The Merlin[®] box then energizes the quadrupole with a certain RF-to-DC ratio to achieve constant peak width across the mass range. The DC and RF voltages are linearly varied to scan a set mass range. The ions filtered by the quadrupole are then fed to the channeltron, thus amplifying the signal. The voltages of the ionizer ion optics are set to maximize the ion transmission. The mass range is scanned 100 times and averaged to minimize noise. Each data set is calibrated using prominent peaks of the calibration substances. After the data collection is completed, the electronics are powered down, the flow of the calibration substance is stopped, and the ionizer is let cool before venting the chamber.

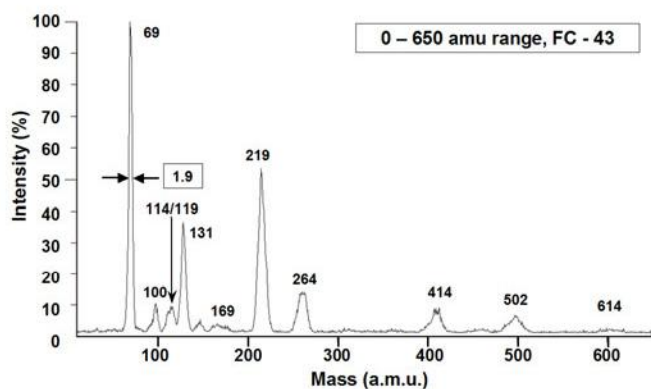


Fig. 9 FC-43 Spectrum

Fig. 9 shows a typical spectrum collected using a 1.44 MHz RF power supply from Pfeiffer Vacuum (Nashua, NH) and a quadrupole with 1.58 mm diameter rods and aspect ratio of 57. Optimization resulted in 13.6 eV ions and a scan rate of 323 amu/s. The mass spectrum contains all the major peaks of FC-43 and shows good agreement in the relative peak intensity with the typical electron ionization spectrum provided by the vendor. However, substantially higher intensity for the larger fragments was observed and the peaks with nominal mass equal to 114 and 119 appear to be overlapped at their bases. The peak widths @ 69-amu and @ 219-amu shows a slight increase with mass, namely from 1.9 amu to 2.2 amu respectively, demonstrating the capability limits of the constant peak width circuit.

6. CONCLUSIONS

We have demonstrated a proof of concept flexible quadrupole platform that uses 3D packaging to implement out-of-plane MEMS quadrupoles with a dynamic range up to 650 amu, and a peak width as small as 2 amu. We have assembled quadrupoles with rod diameter down to 0.56 mm, and driven devices with 1.58 mm rod diameter due to circuit limitations.

ACKNOWLEDGEMENTS

The authors would like to acknowledge the invaluable help of Dr. Randall Pedder of Ardra Technologies (Ardara, PA) in the experimental characterization. The work reported in the paper was sponsored by DARPA/MTO and the US Army Soldier Systems Center (Natick, MA) through contract # W911QY-05-1-0002 (program

managers Clark Nguyen, Dennis Polla and Henry Girolamo). The views and conclusions contained in this document are those of the authors and should not be interpreted as representing the official policies of the U.S. Government.

REFERENCES

- [1] P. Dawson, *Quadrupole Mass Spectrometry and Its Applications*, American Institute of Physics, 1997.
- [2] I. E. Dayton, F. C. Shoemaker, and R. F. Mozley, *The Measurement of Two-dimensional Fields, Part II: Study of a Quadrupole Magnet*, Rev. Sci. Instrum., Vol. 25, pp. 485 – 489, 1954.
- [3] R. J. Ferran and S. Boumsellek, *High-pressure Effects in Miniature Arrays of Quadrupole Analyzers for Residual Gas Analysis from 10⁻⁹ to 10⁻² Torr*, J. Vac. Sci. Technol., Vol A 14 No 3, pp. 1258 – 1265, 1996.
- [4] O. J. Orient, Chutjian A., and Garkanian V. *Miniature, High Resolution, Quadrupole Mass Spectrometer Array*, Rev. Sci. Instrum., vol. 68, pp. 1393 – 1397, 1997.
- [5] R. Syms, T. J. Tate, M. M. Ahmad, and S. Taylor, *Design of a Microengineered Electrostatic Quadrupole Lens*, IEEE Trans. Electron Devices, Vol. 45, No. 11, pp. 2304 – 2311, 1998.
- [6] M. Gear, R. A. Syms, S. Wright, and A. S. Holmes, *Monolithic MEMS Quadrupole Mass Spectrometers by Deep Silicon Etching*, J. Microelectromech. Sys., Vol. 14, No. 5, pp. 1156 – 1166, 2005.
- [7] K. Wark, *“Thermodynamics”*, McGraw Hill, 1991.
- [8] J. R. Gibson and S. Taylor, *Numerical Investigation of the Effect of Electrode Size on the Behavior of Quadrupole Mass Filters*, Rapid Commun. Mass Spectrom., Vol 15, pp. 1960 – 1964, 2001.
- [9] L. F. Velásquez-García, A. I. Akinwande, and M. Martínez-Sánchez, *Precision Hand Assembly of MEMS subsystems using DRIE-patterned Deflection Spring Structures: An Example of an Out-of-plane Substrate Assembly*, accepted, J. Microelectromech. Sys.
- [10] B. Gassend, L. F. Velásquez-García, and A. I. Akinwande, *Hand Assembly of Electrostatic Components with Micron Scale Accuracy*, submitted, J. Microelectromech. Sys.